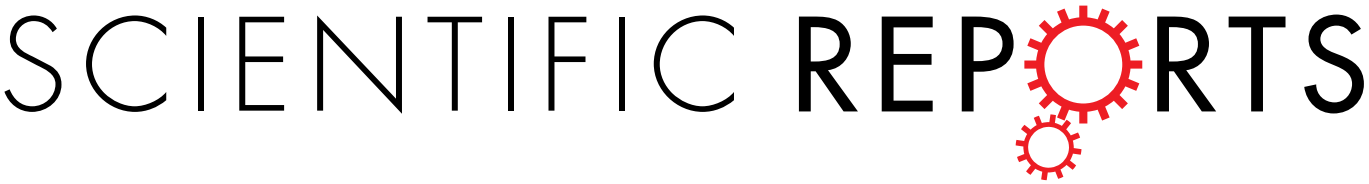

OPEN

Superconductivity in $Ta_3Pd_3Te_{14}$ with quasi-one-dimensional $PdTe_2$ chains

Received: 17 December 2015
Accepted: 26 January 2016
Published: 15 February 2016

Wen-He Jiao[1], Lan-Po He[2], Yi Liu[3], Xiao-Feng Xu[4], Yu-Ke Li[4], Chu-Hang Zhang[1], Nan Zhou[4], Zhu-An Xu[3,5], Shi-Yan Li[2,5] & Guang-Han Cao[3,5]

We report bulk superconductivity at 1.0 K in a low-dimensional ternary telluride $Ta_3Pd_3Te_{14}$ containing edge-sharing $PdTe_2$ chains along crystallographic *b* axis, similar to the recently discovered superconductor $Ta_4Pd_3Te_{16}$. The electronic heat capacity data show an obvious anomaly at the transition temperature, which indicates bulk superconductivity. The specific-heat jump is $\Delta C/(\gamma_n T_c) \approx 1.35$, suggesting a weak coupling scenario. By measuring the low-temperature thermal conductivity, we conclude that $Ta_3Pd_3Te_{14}$ is very likely a dirty *s*-wave superconductor. The emergence of superconductivity in $Ta_3Pd_3Te_{14}$ with a lower T_c, compared to that of $Ta_4Pd_3Te_{16}$, may be attributed to the lower density of states.

Superconductivity (SC) in low-dimensional systems attracts sustained attention in SC community. The discovery of first layered cuprate superconductor $(La, Ba)_2CuO_4$[1], has set off a wave of exploring high-T_c superconductors. Since after, a number of new superconductors with low dimensional structures, such as quasi-two-dimensional (Q2D) strontium ruthenate[2], ferroarsenides[3], bismuth oxysulfides[4], quasi-one-dimensional (Q1D) transition-metal chalcogenides[5], ternary tellurides[6,7], and newly discovered chromium-based compounds[8], were reported to display the features of novel SC. The spin (charge) fluctuations[9,10], strong electron-electron correlations[11], or metal-insulator boundaries[12] among low-dimensional systems constitute the newly strategic prerequisites to explore high-T_c superconductors. Generally, the presence of some transition metal elements among them, which bear strong electron correlations, are believed to play a significant role in producing the exotic pairing glue.

Owing to the inherent nature of transition metal chalcogenides[13], the low-dimensional structures and rich physical properties, e.g., density-wave instability[14], thermoelectricity[15], and SC[5], are prevalent among them. The tellurides, as compared with sulfides or selenides, are quite special in terms of its structures and properties because of the diffuse nature of the tellurium orbitals, and thus far rarely studied. Recently, we reported the observation of SC with $T_c = 4.6$ K in a ternary telluride $Ta_4Pd_3Te_{16}$ with Q1D $PdTe_2$ chains[6]. The detailed studies of its pairing symmetry were followed in applying the techniques of scanning tunneling microscopy[16], low-temperature heat capacity[17] and thermal conductivity[18]. The results indicate an anisotropic gap structure with the possible presence of nodes, although electronic structure calculations show the contributions of Pd 4*d* electrons to the density of states at Fermi level are pretty small[19].

From a crystal-structure viewpoint, $Ta_4Pd_3Te_{16}$ also belongs to a layered compound resulting from the condensation of Pd-based octahedral chains, Ta-based bicapped trigonal prismatic chains, and Ta-based *double* octahedral chains[6,20]. If the Ta-based *double* octahedral chains are replaced by Ta-based *single* octahedral chains, the condensation of the three different types of chains would form the atomic layer of a new compound $Ta_3Pd_3Te_{14}$, which was firstly synthesized by Liimatta and Ibers in 1989[21]. The major difference between them in structure is well reflected from Fig. 1(f), which shows the projection view of one atomic layer of $Ta_3Pd_3Te_{14}$ and $Ta_4Pd_3Te_{16}$ along the *b* axis. The structural details of $Ta_3Pd_3Te_{14}$ are discussed below. Then, considering the close structural relationship of this material with the superconductor $Ta_4Pd_3Te_{16}$, a natural question is whether the former is as well a superconductor.

[1]Department of Physics, Zhejiang University of Science and Technology, Hangzhou 310023, China. [2]State Key Laboratory of Surface Physics, Department of Physics, and Laboratory of Advanced Materials, Fudan University, Shanghai 200433, China. [3]Department of Physics, Zhejiang University, Hangzhou 310027, China. [4]Department of Physics, Hangzhou Normal University, Hangzhou 310036, China. [5]Collaborative Innovation Centre of Advanced Microstructures, Nanjing 210093, China. Correspondence and requests for materials should be addressed to W.-H.J. (email: whjiao@zust.edu.cn) or S.-Y.L. (email: shiyan_li@fudan.edu.cn)

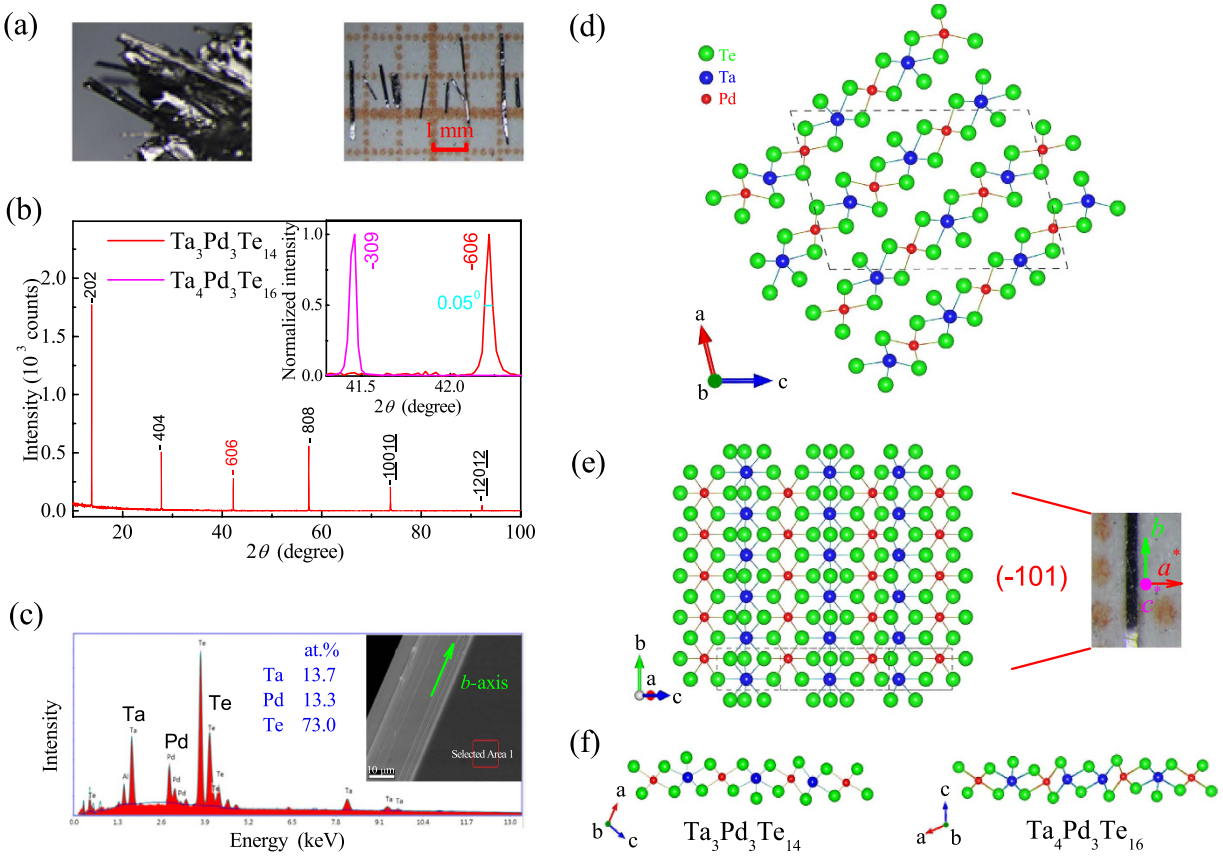

Figure 1. Sample characterization and crystallographic structure of $Ta_3Pd_3Te_{14}$. (**a**) Morphology of a batch of the as-grown $Ta_3Pd_3Te_{14}$ crystals under an optical microscope (left panel) and photographs of the crystals on a millimeter-grid paper (right panel). (**b**) Single-crystal X-ray diffraction pattern. The inset shows the third inflections in X-ray diffraction pattern for both $Ta_3Pd_3Te_{14}$ and $Ta_4Pd_3Te_{16}$. (**c**) A typical energy-dispersive X-ray spectrum with electron beams focused on the selected area (marked in the inset) of the crystals. A small amount of the element Al comes from the sample holder. (**d**) Crystal structure of $Ta_3Pd_3Te_{14}$ projected along the [010] direction. An individual layer of $Ta_3Pd_3Te_{14}$ is shown in the left panel of (**e**). The right panel of (**e**) is a piece of needle-like $Ta_3Pd_3Te_{14}$ crystal under an optical microscope, from which the layered morphology can be clearly identified. (**f**) Projection view of one atomic layer of $Ta_3Pd_3Te_{14}$ (left) and $Ta_4Pd_3Te_{16}$ (right) along the *b* axis.

In this paper, we report the observation of SC with $T_c = 1.0$ K in layered ternary telluride $Ta_3Pd_3Te_{14}$ with Q1D $PdTe_2$ chains. The bulk SC was identified by the electronic heat capacity data, which shows an obvious anomaly at the transition temperature. The specific-heat jump $\Delta C/(\gamma_n T_c) \approx 1.35$ indicates $Ta_3Pd_3Te_{14}$ may be a weakly coupled superconductor. In addition, the result of low-temperature thermal conductivity measurements of $Ta_3Pd_3Te_{14}$ crystal down to 80 mK suggests a dirty *s*-wave superconducting gap. We summarize our results by discussing the similarities and differences between the closely related superconductors of $Ta_3Pd_3Te_{14}$ and $Ta_4Pd_3Te_{16}$, and compiled an extended list of their physical properties.

Results

Single crystals of $Ta_3Pd_3Te_{14}$ were grown using a self-flux method, rather than the vapor transport method previously used[21]. Shiny flattened needle-like crystals with a typical size of $2 \times 0.15 \times 0.1$ mm^3 were harvested, as shown in Fig. 1(a). The X-ray diffraction (XRD) pattern at 298 K by a conventional θ-2θ scan for the crystals lying on a sample holder is shown in Fig. 1(b), in which we can observe only multiple peaks arising from the diffraction from ($\bar{1}$ 0 1) planes, consistent with the layered crystal structure of $Ta_3Pd_3Te_{14}$. $Ta_3Pd_3Te_{14}$ crystalizes in space group $P2_1/m$ with a monoclinic unit cell of $a = 14.088(19)$ Å, $b = 3.737(3)$ Å, $c = 20.560(19)$ Å, and $\beta = 103.73(5)°$ at 123 K[21]. As seen in Fig. 1(d), the layered slabs compose of successively six different chains of three different types. The three types of chains are Ta-based bicapped trigonal prismatic chains, Pd-based octahedral chains, and Ta-based octahedral chains, respectively. The arrangement of the chains, in such a way that every Pd-based chain has two adjacent Ta-based chains and vice versa, constitute the layered slab as clearly depicted in Fig. 1(e). For simplicity, hereafter we define the a^* axis as to be parallel to the[1 0 1] direction and the c^* axis as to be perpendicular to the ($\bar{1}$ 0 1) plane. The interplane spacing at room temperature is determined to be 6.418 Å, and this value is well consistent with the calculated one of 6.397 Å using the above mentioned parameters at 123 K, when taking into account the temperature difference. To compare the obvious difference of the interlayer spacing of $Ta_3Pd_3Te_{14}$ and $Ta_4Pd_3Te_{16}$, we plot the third reflection together, namely (−606) and (−309) peaks, in the inset of Fig. 1(b), from which one can easily find the interplane spacing of $Ta_3Pd_3Te_{14}$ is ~2% smaller than that of $Ta_4Pd_3Te_{16}$, and

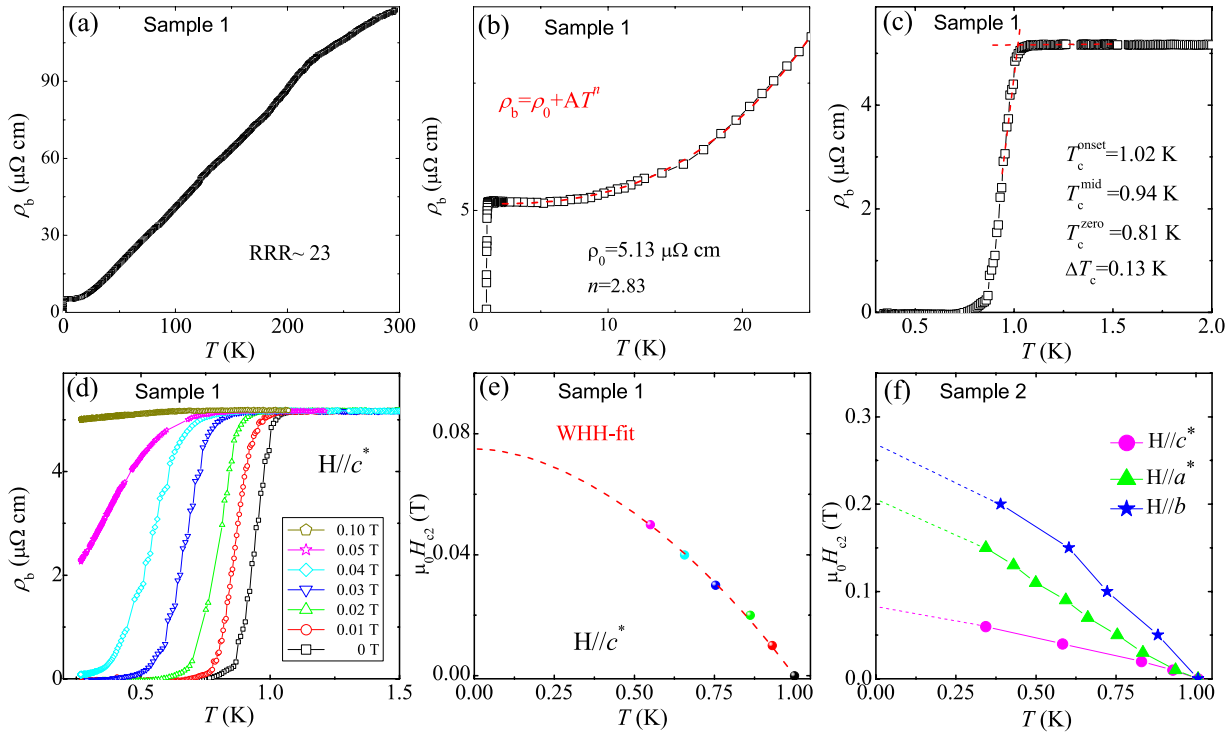

Figure 2. Electrical transport and superconducting phase-diagram. (**a**) Temperature dependence of electronic resistivity of $Ta_3Pd_3Te_{14}$ crystal (Sample 1) along the *b* axis. (**b**) shows the power-law fit to $\rho_b = \rho_0 + AT^n$ in the data range of 2 and 25 K. (**c**) zooms into the low-temperature range to clearly show the superconducting transition. (**d**) The low-temperature resistivity in fields H || c^* up to 0.1 T, from which the upper critical field (H_{c2}) is derived. (**e**) The red dashed line represents the Werthamer-Helfand-Hohenberg (WHH) fitting. (**f**) The extracted upper critical field H_{c2} of $Ta_4Pd_3Te_{16}$ crystal (Sample 2) for different field orientations.

full width at half-maximum is only 0.05°, indicating the high quality of the crystals. The chemical composition determined by an energy-dispersive X-ray spectroscopy (EDS), are collected in a number of crystals, and the average results confirm that composition of the crystals is the stoichiometric $Ta_3Pd_3Te_{14}$ within the measurement errors. The SEM image, shown in the upper right corner of Fig. 1(c), has a morphology with stripes along the *b* axis (chain direction), consistent with the preferential crystal growth along the chain direction.

Figure 2(a) shows temperature dependence of electronic resistivity along the *b* axis (ρ_b) for the $Ta_3Pd_3Te_{14}$ crystal (Sample 1). The larger room temperature resistivity (1.18 $\mu\Omega$ m), than that (0.61 $\mu\Omega$ m) of $Ta_4Pd_3Te_{16}$[6], indicates $Ta_3Pd_3Te_{14}$ is less conductive, consistent with the previous reports[21,22]. The temperature dependence of resistivity shows a metallic behavior without any obvious anomaly down to $T_c = 1.0$ K, at which a sharp superconducting transition appears, as clearly depicted in Fig. 2(c). The value of T_c is 3.6 K less than that of $Ta_4Pd_3Te_{16}$. The onset, midpoint, and zero-resistance temperatures are 1.02 K, 0.94 K, and 0.81 K, respectively, and the superconducting transition width ΔT_c is 0.13 K. The $\rho_b(T)$ data between 2 and 25 K can be well fitted by to $\rho_b = \rho_0 + AT^n$, giving a residual resistivity $\rho_0 = 5.13\,\mu\Omega$ cm and $n = 2.83$ [Fig. 2(b)]. The value of *n* more than 2 was also observed in $Ta_4Pd_3Te_{16}$, which was attributed to the phonon-assisted *s-d* interband scattering[18]. The residual resistivity ratio (RRR) is estimated to be RRR = $\rho_b(300\,\text{K})/\rho_0 \sim 23$, similar to that of $Ta_4Pd_3Te_{16}$ (see Table 1).

Figure 2(d) plots the low-temperature resistivity of $Ta_3Pd_3Te_{14}$ crystal (Sample 1) for H || c^* up to 0.1 T. Upon increasing the field, the superconducting transition is suppressed to lower temperature. The extracted upper critical fields $H_{c2}(T)$ for H || c^*, determined by using 90% criterion, *i.e.*, the field at which ρ_b reaches 90% of the normal state resistivity, are shown in Fig. 2(e). We applied the isotropic one-band Werthamer-Helfand-Hohenberg (WHH) formalism to roughly estimate H_{c2}[23]. As can be seen in Fig. 2(e), H_{c2} for H || c^* is estimated to be 0.075 T at zero temperature with the derived Maki parameter $\alpha = 1.7$ and spin-orbit coupling parameter $\lambda_{so} = 1.2$. However, by employing the orbital limiting field $\mu_0 H_{c2}^{orb}(0) = -0.69\mu_0(dH_{c2}/dT)_{T_c} T_c = 0.1$ T in WHH model and the BCS Pauli-limiting field $\mu_0 H_P^{BCS} = 1.84 T_c = 1.84$ T, the Maki parameter $\alpha = \sqrt{2}\,H_{c2}^{orb}(0)/H_P^{BCS}$ is calculated to be 0.077. This inconsistence between the calculated value of α and the fitted one may originate from the anisotropic effect in $Ta_3Pd_3Te_{14}$. The extracted H_{c2} with fields applied along a^*, *b*, and c^* directions for Sample 2 are shown in Fig. 2(f), and the resistivity data of Sample 2 are not shown here. By roughly linear extrapolations, the anisotropic H_{c2} at zero temperature are estimated to be 0.21, 0.27 and 0.086 T for the a^*, *b* and c^* directions. Using the Ginzburg-Landau formula, the superconducting coherence length ξ are calculated to be 545, 703 and 223 Å for a^*, *b* and c^* directions, respectively, which are much larger than those of its analog $Ta_4Pd_3Te_{16}$[17]. The SC in $Ta_3Pd_3Te_{14}$ is anisotropic but as well three-dimensional in nature, similar to other superconductors with Q1D

Space group	$Ta_3Pd_3Te_{14}$ $P2_1/m$	$Ta_4Pd_3Te_{16}$ $I2/m$
Physical parameters		
RRR	23	26
T_c (K)	1.0	4.6
ΔT_c (K)	0.13	0.76
$\mu_0(dH_{c2}/dT)_{T_c}$ (T/K) $(\boldsymbol{H}\|\|c^*)$	−0.14	−0.44
$\mu_0 H_{c2}$ (T) $(\boldsymbol{H}\|\|c^*)$	0.075	3.3
γ_n (mJ mol^{-1} K^{-2})	28.2	46.1
θ_D (K)	151.6	148.8
λ_{ph}	0.51	0.77
λ_{nph}	1.99	1.53[6], 0.12[19]
$N_{bs}(E_F)$ (eV^{-1} fu^{-1})	3.4[20]	9.6[19], 5.5[20]
$\Delta C/(\gamma_n T_c)$	1.35	1.40

Table 1. Comparison of some physical parameters of the superconductors $Ta_3Pd_3Te_{14}$ (present work and[20]) and $Ta_4Pd_3Te_{16}$[6,17,19,20]. RRR, T_c, ΔT_c, H_{c2}, γ_n, θ_D, λ_{ph}, λ_{nph}, $N_{bs}(E_F)$, and $\Delta C/(\gamma_n T_c)$ denote the residual resistivity ratio, superconducting transition temperature, transition width, upper critical field, electronic specific-heat coefficient, Debye temperature, electron-phonon coupling constant, electron-nonphonon coupling constant, density of states at Fermi level, and dimensionless specific-heat jump, respectively.

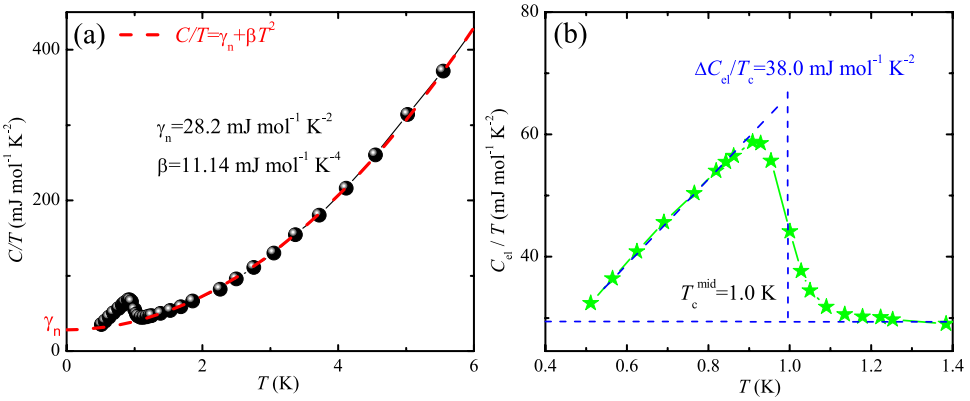

Figure 3. Temperature dependence of specific heat. (**a**) C/T vs T, in which the red dashed line represents the fit with the formula $C/T = \gamma_n + \beta T^2$ for the normal-state data from 1.2 to 6.5 K. (**b**) The electronic specific heat divided by temperature C_{el}/T in the superconducting state, where $C_{el} = C - \beta T^3$.

characteristics, *e.g.*, $Ta_4Pd_3Te_{16}$[17], $Nb_3Pd_{0.7}Se_7$[24], and $Nb_2Pd_xSe_5$[25], since the interchain coherence length ξ^{a^*} and ξ^{c^*} are much larger than the distance between two arbitrarily adjacent chains.

The low-temperature specific heat data of $Ta_3Pd_3Te_{14}$ crystals, plotted as C/T vs T, are shown in Fig. 3(a). We fit the normal-state data from 1.2 to 6.5 K, employing the usual formula $C/T = \gamma_n + \beta T^2$, which is represented as the red dashed line. The fitting yields an electronic heat capacity coefficient $\gamma_n = 28.2 \pm 0.9$ mJ mol^{-1} K^{-2}, and a phononic coefficient $\beta = 11.14 \pm 0.04$ mJ mol^{-1} K^{-4}. The calculated Debye temperature $\Theta_D = 151.6$ K is close to the value of $Ta_4Pd_3Te_{16}$, consistent with the fact that the structures of two tellurides are closely related. However, the value of extracted coefficient γ_n is nearly 40% smaller than that of $Ta_4Pd_3Te_{16}$[17]. Using the relation $N(E_F) = 3\gamma_n/k_B^2\pi^2$ for noninteracting electron systems, where k_B is the Boltzmann constant, we estimated the density of states at the Fermi level $N(E_F)$ to be about 11.9 ± 0.8 eV^{-1} fu^{-1}, which is 3.5 times that of the bare density of states $N_{bs}(E_F)$, obtained from the previous band-structure calculations[20]. Therefore, the larger renormalization factor $[N(E_F)/N_{bs}(E_F) = 1 + \lambda]$, than that for $Ta_4Pd_3Te_{16}$, suggests much stronger electron-electron correlations in $Ta_3Pd_3Te_{14}$, although the recent band-structure calculations are concluded with a higher $N_{bs}(E_F) = 9.6$ eV^{-1} fu^{-1} for $Ta_4Pd_3Te_{16}$, thus resulting in a much lower renormalization factor[19]. To extract the electron-nonphonon coupling strength λ_{nph} in λ, we estimate the electron-phonon coupling constant λ_{ph} by employing the McMillan formula[26], $\lambda_{ph} = [1.04 + \mu^* \ln(\Theta_D/1.45T_c)]/[(1 - 0.62\mu^*)\ln(\Theta_D/1.45T_c) - 1.04]$, where the Coulombic repulsion parameter μ^* is empirically set to be 0.13. The estimated value of λ_{ph} is 0.51, a little bit smaller than that of the superconductor $Ta_4Pd_3Te_{16}$[6]. However, the resultant constant $\lambda_{nph} = \lambda - \lambda_{ph} = 1.99$ is much larger than that of $Ta_4Pd_3Te_{16}$, possibly indicating much larger electron correlations in the former compound.

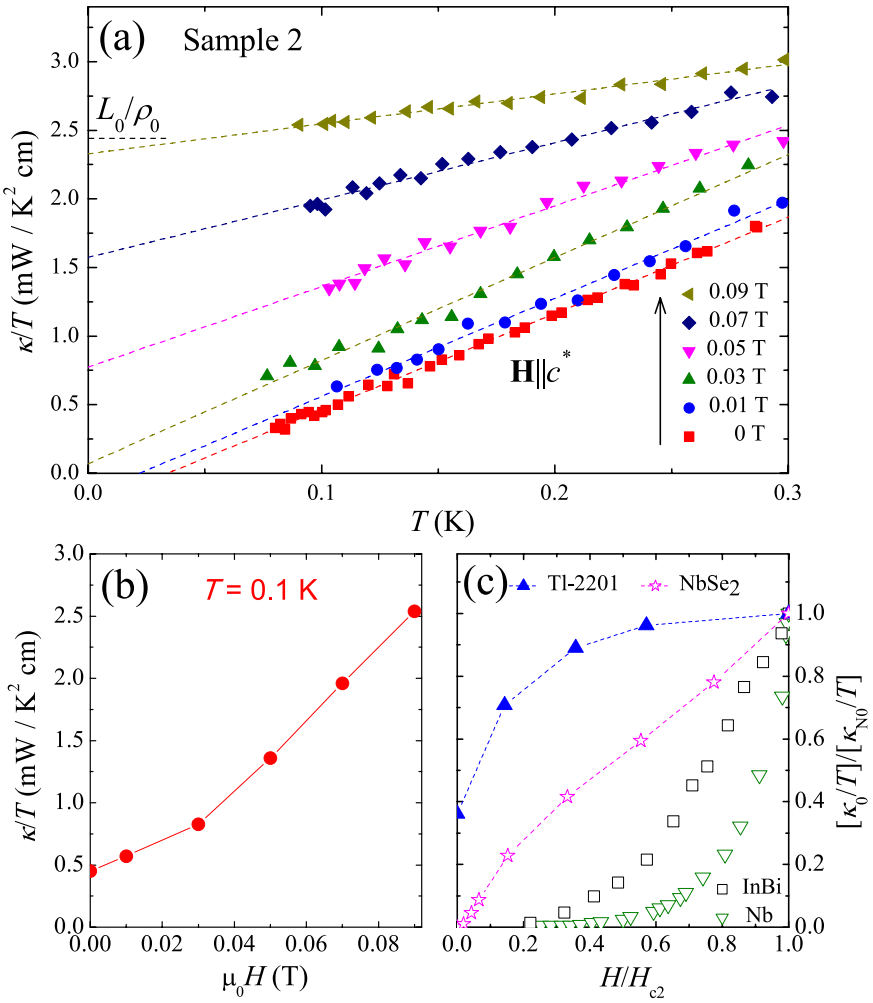

Figure 4. Low-temperature thermal conductivity data. (**a**) Low-temperature thermal conductivity of $Ta_3Pd_3Te_{14}$ crystal (Sample 2) in zero and magnetic fields applied along c^* direction. The dashed lines are fits to the formula $\kappa/T = \kappa_0/T + bT$. The black dashed line is the normal-state Wiedemann-Franz law expectation L_0/ρ_0. (**b**) The field dependence of κ/T at 0.1 K. (**c**) Normalized residual linear term κ_0/T as a function of normalized field H/H_{c2} for the clean *s*-wave superconductor Nb[36], the dirty *s*-wave superconducting alloy InBi[32], the multi-band *s*-wave superconductor $NbSe_2$[37], and an overdoped *d*-wave cuprate superconductor Tl-2201[38].

Discussion

We discuss the electronic heat capacity C_{el} of $Ta_3Pd_3Te_{14}$ crystals in low-temperature range, obtained by $C_{el} = C - \beta T^3$. As can be seen in Fig. 3(b), a characteristic superconducting jump (ΔC_{el}) shows up around ~1 K, confirming the bulk SC. The $\Delta C_{el}/T_c$ is estimated to be 38.0 mJ mol^{-1} K^{-2} and the midpoint temperature of the thermodynamic transition is 1.0 K, consistent with the superconducting transition in low-temperature resistivity. The dimensionless specific-heat jump can be calculated to be 1.35, smaller than the theoretical value (1.43) of the well-known BCS theory, indicating $Ta_3Pd_3Te_{14}$ may be a weakly coupled superconductor. Unfortunately, due to the insufficient data points, we are unable to fit $\Delta C_{el}(T)$ with standard gap functions to give valuable information about the gap symmetry.

To shed light on the superconducting gap structure, we measured the thermal conductivity of $Ta_3Pd_3Te_{14}$ single crystal (Sample 2) in zero and magnetic fields (along c^* direction), the results of which are plotted as κ/T vs T in Fig. 4(a). Since all the curves presented in Fig. 4(a) are roughly linear as previously reported in $Ta_4Pd_3Te_{16}$[18] and some iron-based superconductors[27,28], we fit all the curves to $\kappa/T = a + bT^{\alpha-1}$ by fixing α to 2. The two terms aT and bT^{α} represent contributions from electrons and phonons, respectively[29,30]. From the curve in magnetic field $H = 0.09$ T, which is close to the critical field $H_{c2}(0)$ for $\boldsymbol{H} \| c^*$, one can see that the obtained κ_0/T roughly meets the normal-state Wiedemann-Franz law expectation $\kappa_{N0}/T = L_0/\rho_0 = 2.44$ mW K^{-2} cm^{-1}. Here, L_0 is the Lorenz number 2.45×10^{-8} W Ω K^{-2} and $\rho_0 = 10.04\,\mu\Omega$ cm is the residual resistivity of Sample 2. The verification of the Wiedemann-Franz law in the normal state demonstrates that our thermal conductivity measurements are reliable. For the curves in $H = 0$ and 0.01 T, however, the linear fittings give two negative values, $\kappa_0/T = -0.24$ and -0.16 mW K^{-2} cm^{-1}, respectively. These negative κ_0/T have no physical meaning, just because the temperature

of our measurement is not low enough, comparing to the T_c. Down to lower temperature, the curve in zero field should deviate from the linear behavior.

Since we can not extrapolate κ_0/T at low field, we plot the field dependence of κ/T at $T = 0.1$ K, well below T_c, in Fig. 4(b) to get more information about the superconducting gap structure of $Ta_3Pd_3Te_{14}$[31]. One can see that the increase of κ/T at low field is rather slow, and the curve is similar to that of dirty *s*-wave superconduting alloy InBi[32], which is shown in Fig. 4(c). By using the estimated value of the coherence length ξ along *b* direction, the formula $\xi = 0.18\hbar v_F/k_B T_c$ gives the Fermi velocity $v_F = 5.11 \times 10^4$ m s^{-1} [33]. Then, according to the relationship $\kappa_{N0}/T = \gamma_n v_F l_e/3$, the electron mean free path is estimated to be $l_e = 322$ Å, which is much smaller than the *b*-direction ξ. This result indicates $Ta_3Pd_3Te_{14}$ is indeed in the dirty limit. Therefore, it is concluded that $Ta_3Pd_3Te_{14}$ is very likely a dirty *s*-wave superconductor.

It is instructive to compare the physical properties of the two structural closely related compounds of $Ta_3Pd_3Te_{14}$ and $Ta_4Pd_3Te_{16}$, which we summarize in Table 1. Both of the two tellurides show Q1D characteristic with Q1D $PdTe_2$ chains. The larger RRR could account for the much sharper superconducting transition for $Ta_3Pd_3Te_{14}$. Although T_c of $Ta_3Pd_3Te_{14}$ is 3.6 K less than that of $Ta_4Pd_3Te_{16}$, the former compound show much stronger electron correlations, verified by the larger renormalization factor and larger electron-nonphonon coupling strength λ_{nph}. The small values of both $\Delta C/(\gamma_n T_c)$ and λ_{ph} indicate $Ta_3Pd_3Te_{14}$ is a weakly coupled superconductor. In addition, if assuming the Drude model, in which the electron-electron interactions are neglected, is applicable, a superconductor is expected to have a lower T_c for a lower value of Sommerfield coefficient γ_n, which in this case signifies the lower density of states at Fermi level. This simple conclusion is compatible with the general trend for the above two superconductors. Therefore, the lower T_c in the title compound, may be attributed to the lower density of states at Fermi level. In this sense, by tuning the Fermi level of $Ta_3Pd_3Te_{14}$ or $Ta_4Pd_3Te_{16}$ by the way of doping or proper intercalations, the value of T_c may be enhanced. By the way, in recently discovered PdTe or PdS chains based superconductors, there have been several pieces of work that show the evidences of two-gap SC[17,34,35]. However, our results presented above indicate the new superconductor $Ta_3Pd_3Te_{14}$ with $PdTe_2$ chains is very likely a fully gapped *s*-wave one. We have previously reported that $Ta_4Pd_3Te_{16}$ is possibly a two-gap superconductor with a gap symmetry of $s + d$ waves[17]. Thus, if assuming the reduced part of electronic states at the Fermi level in $Ta_3Pd_3Te_{14}$, compared to that in $Ta_4Pd_3Te_{16}$, is primarily due to the reduced contribution from the Pd *d* states, it would be reasonable to see only a *s*-wave gap left in the former compound.

Methods

Powders of the elements Ta (99.97%), Pd (99.995%) and Te (99.99%) with a ratio of Ta : Pd : Te = 2 : 3 : 10 were thoroughly mixed together, loaded, and sealed into an evacuated quartz ampule. The sample-loaded quartz ampoule is then heated to 1223 K, held for 24 h, and cooled to 723 K at a rate of 5 K/h, followed by furnace cooling to room temperature. The above procedures are similar to that in growing $Ta_4Pd_3Te_{16}$ crystals[6]. The chemical composition is checked by an EDS with an AMETEK EDAX (Model Octane Plus) spectrometer, equipped in a field-emitting scanning electron microscope (SEM, Hitachi S-4800). It is worthy to mention that, although one may speculate the as-grown $Ta_3Pd_3Te_{14}$ crystals should be mixed by the $Ta_4Pd_3Te_{16}$ crystals in the same batch, our results do not support this speculation. The reasons are as follows: Using this method and atomic ratio of Ta : Pd : Te = 2 : 3 : 10 to grow $Ta_3Pd_3Te_{14}$ crystals, $Ta_4Pd_3Te_{16}$ crystals were occasionally harvested. However, our results show that the two kinds of crystals are never mixed with each other in the same batch. This conclusion is drawn by the fact that once the crystals, randomly picked up from the final product in one batch, are checked by both XRD and EDS to be $Ta_3Pd_3Te_{14}$, not a single piece of $Ta_4Pd_3Te_{16}$ crystals can be identified in the same batch, and vise versa.

The magnetoresistance (MR) measurements were carried out in a ^{3}He cryostat down to 0.27 K by a stand four-probe technique with current applied along the *b* axis. The specific heat for a bundle of shiny needle-like crystals with a total mass $m = 1.30(2)$ mg was measured by a long relaxation method utilizing a commercial ^{3}He microcalorimeter (Quantum Design PPMS-9). The thermal conductivity was measured in a commercial dilution refrigerator, using a standard four-wire steady-state method with two RuO_2 chip thermometers, calibrated *in situ* against a reference RuO_2 thermometer. The chemical composition of the crystals employed for above measurements have also been checked to be $Ta_3Pd_3Te_{14}$ by both XRD and EDS.

References

1. Bednorz, J. G. & Müller, K. A. Possible high T_c superconductivity in the BaLaCuO system. *Z. Phys. B* **64,** 189 (1986).
2. Maeno, Y. *et al.* Superconductivity in a layered perovskite without copper. *Nature* **372,** 532 (1994).
3. Kamihara, Y., Watanabe, T., Hirano, M. & Hosono, H. Iron-based layered superconductor $La[O_{1-x}F_x]FeAs$ ($x = 0.05$–0.12) with $Tc = 26$ K. *J. Am. Chem. Soc.* **130,** 3296 (2008).
4. Mizuguchi, Y. *et al.* BiS_2-based layered superconductor $Bi_4O_4S_3$. *Phys. Rev. B* **86,** 220510(R) (2012).
5. Zhang, Q. *et al.* Superconductivity with extremely large upper critical fields in $Nb_2Pd_{0.81}S_5$. *Sci. Rep.* **3,** 1446 (2013).
6. Jiao, W. H. *et al.* Superconductivity in a layered $Ta_4Pd_3Te_{16}$ with $PdTe_2$ chains. *J. Am. Chem. Soc.* **136,** 1284 (2014).
7. Goyal, R., Tiwari B., Jha, R. & Awana, V. P. S. Superconductivity at 4.4 K in $PdTe_2$-chains of a Ta based compound. *J. Supercond. Nov. Magn.* **28,** 1195 (2015).
8. Bao, J. K. *et al.* Superconductivity in quasi-one-dimensional $K_2Cr_3As_3$ with significant electron correlations. *Phys. Rev. X* **5,** 011013 (2015).
9. Stewart, G. R. Superconductivity in iron compounds. *Rev. Mod. Phys.* **83,** 1589 (2011).
10. Yasuhiro, T., Youichi, Y. & Masao, O. Superconductivity in $Na_xCoO_2{\cdot}yH_2O$ due to charge fluctuation. *J. Phys. Soc. Jpn.* **73,** 319 (2004).
11. Lee, P. A., Nagaosa, N. & Wen, X. G. Doping a mott insulator: Physics of high-temperature superconductivity. *Rev. Mod. Phys.* **88,** 033620 (2013).
12. Lefebvre, S. *et al.* Mott transition, antiferromagnetism, and unconventional superconductivity in layered organic superconductors. *Phys. Rev. Lett.* **85,** 5420 (2000).
13. Mitchell, K. & Ibers, J. A. Rare-earth transition-metal chalcogenides. *Chem. Rev.* **102,** 1929 (2002).
14. Wilson, J. A., Di Salvo, F. J. & Mahajan, S. Charge-density waves and superlattices in the metallic layered transition metal dichalcogenides. *Adv. Phys.* **24,** 117 (1975).

15. Tritt, T. M. Holey and unholey semiconductors. *Science* **283,** 804 (1999).
16. Du, Z. Y. *et al.* Anisotropic superconducting gap and elongated vortices with caroli-de gennes-matricon states in the new superconductor $Ta_4Pd_3Te_{16}$. *Sci. Rep.* **5,** 9408 (2015).
17. Jiao, W. H. *et al.* Multiband superconductivity in $Ta_4Pd_3Te_{16}$ with anisotropic gap structure. *J. Phys.*: *Cond. Matt.* **27,** 325701 (2015).
18. Pan, J. *et al.* Nodal superconductivity and superconducting dome in the layered superconductor $Ta_4Pd_3Te_{16}$. *Phys. Rev. B* **92,** 180505(R) (2015).
19. Singh, D. J. Multiband superconductivity of $Ta_4Pd_3Te_{16}$ from Te *p* states. *Phys. Rev. B* **90,** 144501 (2014).
20. Alemany, P., Jobic, S., Brec, R. & Canadell, E. Oxidation states, transport properties, and Te···Te short contacts in the ternary transition metal tellurides $Ta_3Pd_3Te_{14}$ and $Ta_4Pd_3Te_{16}$. *Inorg. Chem.* **36,** 5050 (1997).
21. Liimatta, E. W. & Ibers, J. A. Synthesis, structures, and conductivities of the new layered compounds $Ta_3Pd_3Te_{14}$ and $TaNiTe_5$. *J. Solid State Chem.* **78,** 7 (1989).
22. Mar, A. & Ibers, J. A. Synthesis, crystal structure and electrical conductivity of a new layered ternary telluride $Ta_4Pd_3Te_{16}$. *J. Chem. Soc., Dalton Trans.* **S,** 639 (1991).
23. Werthamer, N. R., Helfand, E. & Hohenberg, P. C. Temperature and purity dependence of the superconducting critical field, H_{c2}. III. Electron spin and spin-orbit effects. *Phys. Rev.* **147,** 295 (1966).
24. Zhang, Q. R. *et al.* Anomalous metallic state and anisotropic multiband superconductivity in $Nb_3Pd_{0.7}Se_7$. *Phys. Rev. B* **88,** 024508 (2013).
25. Khim, S. *et al.* Enhanced upper critical fields in a new quasi-one-dimensional superconductor $Nb_2Pd_xSe_5$. *New J. Phys.* **15,** 123031 (2013).
26. McMillan, W. L. Transition temperature of strong-coupled superconductors. *Phys. Rev.* **167,** 331 (1968).
27. Dong, J. K. *et al.* Quantum criticality and nodal superconductivity in the FeAs-based superconductor KFe_2As_2. *Phys. Rev. Lett.* **104,** 087005 (2010).
28. Qiu, X. *et al.* Robust nodal superconductivity induced by isovalent doping in $Ba(Fe_{1-x}Ru_x)_2As_2$ and $BaFe_2(As_{1-x}P_x)_2$. *Phys. Rev. X* **2,** 011010 (2012).
29. Li, S. Y. *et al.* Low-temperature phonon thermal conductivity of single-crystalline Nd_2CuO_4: Effects of sample size and surface roughness. *Phys. Rev. B* **77,** 134501 (2008).
30. Sutherland, M. *et al.* Thermal conductivity across the phase diagram of cuprates: Low-energy quasiparticles and doping dependence of the superconducting gap. *Phys. Rev. B* **67,** 174520 (2003).
31. Shakeripour, H., Petrovic, C. & Taillefer, L. Heat transport as a probe of superconducting gap structure. *New J. Phys.* **11,** 055065 (2009).
32. Willis, J. O. & Ginsberg, D. M. Thermal-conductivity of superconducting alloy-films in a perpendicular magnetic-field. *Phys. Rev. B* **14,** 1916 (1976).
33. See, for example, Tinkham, M. *Introduction to superconductivity* (McGraw-Hill, New York, 1975).
34. Goyal, R., Tiwari, B., Jha, R. & Awana, V. P. S. Specific heat of robust Nb_2PdS_5 superconductor. *J. Supercond. Nov. Magn.* **28,** 1427 (2015).
35. Park, E. *et al.* Spectroscopic evidence for two-gap superconductivity in the quasi-one dimensional chalcogenide $Nb_2Pd_{0.81}S_5$. Preprinted at http://arxiv.org/abs/1505.01258 (2015).
36. Lowell, J. & Sousa, J. B. Mixed-state thermal conductivity of type II superconductors. *J. Low Temp. Phys.* **3,** 65 (1970).
37. Boaknin, E. *et al.* Heat conduction in the vortex state of $NbSe_2$: Evidence for multiband superconductivity. *Phys. Rev. Lett.* **90,** 117003 (2003).
38. Proust, C., Boaknin, E., Hill, R. W., Taillefer, L. & Mackenzie, A. P. Heat transport in a strongly overdoped cuprate: Fermi liquid and a pure *d*-wave BCS superconductor. *Phys. Rev. Lett.* **89,** 147003 (2002).

Acknowledgements

This work was supported by the Natural Science Foundation of China (Grand Nos 11504329 and 11190023), the National Basic Research Program (No. 2011CBA00103), the Fundamental Research Funds for the Central Universities of China, and Zhejiang Provincial Natural Science Foundation of China (Grand No. LQ15A040005).

Author Contributions

W.H.J., Y.L. and C.H.Z. synthesized the crystals of $Ta_3Pd_3Te_{14}$. W.H.J., X.F.X., Y.K.L. and N.Z. performed transport measurements and heat-capacity measurement. The low-temperature thermal conductivity measurements were performed by L.P.H. W.H.J., S.Y.L., G.H.C. and Z.A.X. analyzed the whole data. W.H.J. and S.Y.L. wrote the main manuscript text. All authors reviewed the manuscript.

Additional Information

Competing financial interests: The authors declare no competing financial interests.

How to cite this article: Jiao, W.-H. *et al.* Superconductivity in $Ta_3Pd_3Te_{14}$ with quasi-one-dimensional $PdTe_2$ chains. *Sci. Rep.* **6**, 21628; doi: 10.1038/srep21628 (2016).